Materials Science and Engineering A 517 (2009) 321–327

Contents lists available at ScienceDirect

Materials Science and Engineering A

journal homepage: www.elsevier.com/locate/msea

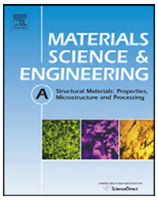

Phase formation in 6060/4043 aluminum weld solidification

N. Coniglio[a], C.E. Cross[b,*], I. Dörfel[b], W. Österle[b]

[a] The University of Adelaide, Adelaide, SA 5005, Australia
[b] Federal Institute for Materials Research and Testing (BAM), 12200 Berlin, Germany

ARTICLE INFO

Article history:
Received 30 January 2009
Received in revised form 27 March 2009
Accepted 31 March 2009

Keywords:
6060 Aluminum
GTA weld
Weld metal microstructure
Cooling rate
Scanning TEM
Thermal analysis

ABSTRACT

Weld metal microstructure for alloy 6060 aluminum welds, made using the gas-tungsten arc process and alloy 4043 filler metal, has been characterized using optical metallography, EPMA microprobe analysis, SEM/EBSD and STEM/EDX electron microscopy, and single-sensor differential thermal analysis (SS-DTA). In addition, alloy 6060 castings were solidified at variable cooling rates approaching that of welding, to provide a reference for comparison with weld microstructure. It was found that a major change in cast microstructure occurs at cooling rates higher than 27 K/s resulting in a structure similar to that observed in weld metal. Rapid cooling is believed to favor low temperature solidification reactions that normally would be achieved only at higher silicon content. Accordingly, additions of 4043 filler metal that increase the weld metal silicon content have only limited affect on weld solidification range and microstructure. This has direct implications regarding how 4043 filler additions improve weldability and weld quality.

1. Introduction

Al–Si–Mg extrusion alloys are widely used in fabricated structures because of their good corrosion resistance, moderate strength, and good weldability, provided that an appropriate filler alloy is used. When welded autogenously, these alloys have been found to be highly susceptible to solidification cracking [1,2]. However, when using an aluminum–silicon filler (e.g. alloy 4043), the weld pool is shifted to a composition with low cracking susceptibility [3,4]. The exact reason behind this improved cracking resistance remains unclear.

To develop a better understanding of weldability requires knowledge of how welds solidify, including solidification path and phase formation. This is particularly important for modeling of weld defect formation (i.e. porosity and solidification cracking) [5,6], based upon the interdendritic pressure drop model of Rappaz et al. [7]. A drop in liquid pressure arises from an inability to feed solidification and thermal shrinkage, which is affected by the solidification range and the nature of the phases present in the mushy zone.

Ternary phase equilibrium for the Al–Si–Mg alloy system is characterized by a quasi-binary occurring at a fixed magnesium–silicon ratio (Mg/Si = 1.73). Alloys that satisfy this ratio (i.e. fixed line on Al–Mg–Si ternary phase diagram) behave like a binary system consisting of α-aluminum and Mg_2Si. Using the quasi-binary as a line of reference, alloys rich in silicon will form Si in addition to Mg_2Si, whereas alloys rich in magnesium will tend to form Mg_5Al_8. The alloys examined in this study, alloy 6060 (0.6 wt.% Mg + 0.4 wt.% Si) welded with 4043 filler metal (5 wt.% Si), reside on the silicon-rich side of this quasi-binary line.

Iron also plays a significant role in aluminum solidification due to its strong tendency to partition (equilibrium partition ratio: $k = 0.03$). While normally present as an impurity in small amounts around 0.2 wt.% (0.3 wt.% Fe max in 6060 extrusions; 0.8 wt.% Fe max in 4043 filler metal), iron tends to form intermetallic compounds with aluminum and silicon, thereby affecting the solidification sequence [8,9]. Phases normally expected when casting an Al–Mg–Si–Fe quaternary alloy like alloy 6060 include ß-Al_5FeSi, α-Al_8Fe_2Si, and π-$Al_8FeMg_3Si_6$ phases in addition to Mg_2Si and Si [10].

The goal of this study was to examine the evolution of alloy 6060 solidification microstructure as a function of cooling rate for different silicon contents representing 4043 dilution. This was achieved by examining 6060 castings made at variable cooling rates approaching that of welding, and comparing this to 6060 weld metal made with and without 4043 filler metal. Phase analysis in weld metal can prove challenging due to the refinement in microstructure that occurs with rapid solidification. By first analyzing slower cooled castings, for which there exists considerable information in the literature, a basis was established for identification of weld metal phases. In the process of doing this, an interesting change in microstructure was observed with increased cooling rate. Several different analytical methods were employed (EBSD, EPMA, STEM, and SS-DTA) to help provide a collective indication of phase identity.

---

* Corresponding author. Tel.: +49 30 8104 1554; fax: +49 30 8104 1557.
E-mail address: carl-edward.cross@bam.de (C.E. Cross).

doi:10.1016/j.msea.2009.03.087

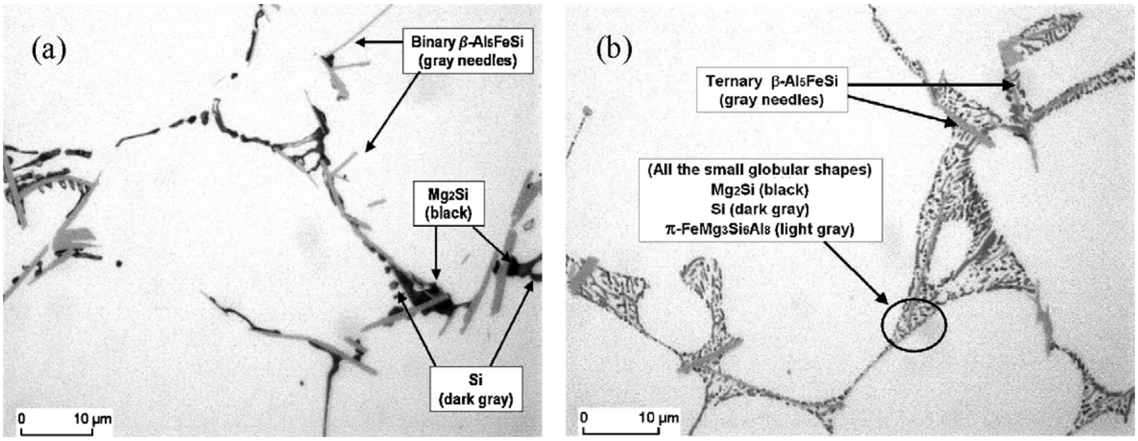

Fig. 1. Comparison of cast structures for (a) 6060, and (b) 6060 + 20% 4043, with the different phases indicated [13]. Cooling rate 13 K/s.

Table 1
Measured chemical analysis for aluminum alloys 6060, 4043, and 6060/4043 mixture (in wt.%).

Alloy	Si	Mg	Fe	Mn	Cu	Cr	Ni	Zn	Ti	Zr
6060	0.42	0.59	0.19	0.02	0.01	0.004	0.004	0.009	0.02	0.001
6060 + 16% 4043	1.20	0.50	0.19	0.02	0.01	0.004	0.004	0.008	0.02	0.001
4043	5.30	0.00	0.22	0.00	0.02	0.002	0.005	0.005	0.00	0.002

2. Background

2.1. Cooling rate effect

Arc welds typically cool at rates (10^1 to 10^2 K/s) much higher than for castings (10^{-1} to 10^0 K/s) depending upon process conditions. This has the effect of producing finer microstructures for welds in terms of reduced grain size and dendrite spacing. Dendrite spacing varies roughly from 100 to 10 µm when comparing castings to arc welds. In particular, the following relationship has been proposed relating dendrite spacing d (in microns) to cooling rate $\mathrm{d}T/\mathrm{d}t$ (in K/s) as applied to alloy 6063 [11]:

$$d = 85(\mathrm{d}T/\mathrm{d}t)^{-0.38} \qquad (1)$$

Accordingly, the size and shape of interdendritic phase constituents must also be affected by cooling rate, limited by diffusion distance and interdendritic dimensions. Also, there is high undercooling associated with weld dendritic solidification due to high temperature gradients and growth rates [12], which can alter the order of phase formation. There is also the possibility that peritectic reactions will become either suppressed or eliminated at high cooling rates, favoring instead eutectic reactions occurring at lower temperature [9].

2.2. Silicon effect

From a previous study [13], the solidification structure for an alloy 6060 casting (13 K/s) is compared in Fig. 1, both without and with 4043 addition. For the case of low silicon (0.42 wt.% Si) in Fig. 1a, coarse ß needles, Mg_2Si particles, and Si plates are clearly discernable along dendrite boundaries. For higher silicon (1.4 wt.% Si) in Fig. 1b, coarse ß needles are seen together with a fine eutectic believed to consist of Mg_2Si, Si, and π particles.

From a thermal analysis of cast 6060/4043 alloy mixtures [13], it was observed that increased silicon favors lower temperature phase reactions and the formation of Si and π phases. The solidification range was found to significantly increase with silicon, as did the quantity of interdendritic eutectic liquid generated, determined using solid fraction versus temperature calculations.

3. Experimental

Solidified mixtures of aluminum alloys 6060 and 4043 have been examined in this study in two different forms, both as castings and as weld metal, in order to vary the silicon content and cooling rate during solidification and compare the resulting microstructures. Specifically, 6060 castings were made at a variable cooling rate, and 6060 welds were made with 0 and 16 wt.% 4043 filler metal. Compositions for alloys 6060, 4043, and the 6060/4043 alloy mixture are compared in Table 1, where it is observed that the addition of 16 wt.% 4043 to alloy 6060 has the primary effect of increasing the silicon concentration by a factor of three in the mixture (i.e. from 0.42 to 1.20 wt.% Si). Magnesium content is reduced only slightly (i.e. from 0.59 to 0.50 wt.% Mg) and other alloying elements remain essentially unaffected.

Castings of alloy 6060 were made in a graphite cylinder mold coated with boron-nitride, using heat sinks attached to the bottom of the cylinder to extract heat at different rates. Heat sink materials included fireclay, stainless steel, and copper. When combined with the use (or absence) of boron-nitride coating on the heat sink, this allowed for a total of 6 different cooling rates to be examined. The graphite mold had an inside diameter of 19 mm, outside diameter of 40 mm, and height of 60 mm. A type-K thermocouple (0.2 mm diameter wire) was placed at the mold center, 30 mm from the heat sink, to monitor the cooling rate during solidification. The molten alloy was superheated to 780 °C and the oxide skimmed prior to casting.

Gas-tungsten arc welds, 120 mm in length, were made on 6060 extruded bars (40 mm wide × 120 mm long × 4 mm thick) in the extrusion direction. Partial penetration welds were made bead-on-plate with 0 and 16 wt.% 4043 filler dilution (0.8 mm wire diameter, 42 mm/s feed rate) and welding parameters summarized in Table 2. Thermal analysis of welds was accomplished by

Table 2
Gas-tungsten arc welding parameters.

Current	Voltage	Polarity	Travel speed	Gas
110 A	18 V	DCEN	4 mm/s	He

plunging a sheathed, electrically grounded, type-K thermocouple (0.5 mm outer diameter) into the weld pool during welding, at weld mid-length. The thermocouple output was recorded at a 200 Hz frequency during solidification using *CATMAN*$^{\text{TM}}$ *4.5* computer software for data acquisition and a *Spider*$^{\text{TM}}$ *8* analog-to-digital converter.

Two different thermal analysis methods were used to characterize the solidification of the 6060/4043 alloy welds: cooling rate method and SS-DTA method. The first method follows from work done by Bäckerud et al. for aluminum castings [14], and the second from Alexandrov and Lippold for welds [15], both founded on the principle that thermal arrests observed during cooling correspond to phase formation and the release of latent heat. The cooling rate method serves to identify thermal arrests by examining the first derivative of the cooling curve. The SS-DTA method identifies arrests by comparing the measured cooling curve with a curve-fit approximation of the cooling curve, and then examining the first derivative of the difference.

Specimens sectioned from castings and welds were prepared for metallographic analysis by grinding and polishing to 1 μm followed by chemical polishing using a slightly basic solution of colloidal silicon dioxide. Optical examination of specimens occurred in the un-etched condition. Weld metal and casting grain size was measured with the aid of SEM/EBSD to differentiate grains by orientation using a LEO$^{\text{TM}}$ Gemini 1530 VP machine. EPMA microprobe analysis was performed on deep-etched specimens using a JEOL-Microbeam JXA-8900 RL. Deep-etching in caustic solution (1% NaOH, 10 min at 60 °C) preferentially attacked the aluminum matrix and provided surface relief for improved particle access. Scanning and diffraction TEM analysis was performed using a JEOL$^{\text{TM}}$ JEM-2200FS, with the TEM specimens prepared using a FEI$^{\text{TM}}$ Strata 200 xP type Focused ion beam (FIB).

4. Results and discussion

4.1. Comparison of cooling rates

A comparison of solidification cooling curves for cast alloy 6060 is provided in Fig. 2, showing average cooling rates between 6 and 50 K/s, measured between 750 and 500 °C. Also included is a cooling curve for the 6060 gas-tungsten arc weld measured to be 54 K/s (i.e. close to the fastest cooled casting). One important observation to be made here is that the recalescence plateau, associated with aluminum dendrite formation, is gradually diminished for increased cooling rates. For the castings, this reflects upon a fixed quantity of latent heat being removed at increasingly higher rates, corresponding to a reduced local solidification time. In the case of the weld, with a smaller liquid volume and quantity of latent heat, a plateau is not observed at all. Specifically, the solidification time for these castings is found to descend from approximately 17 to 3 s for the slowest to the fastest cooling rate.

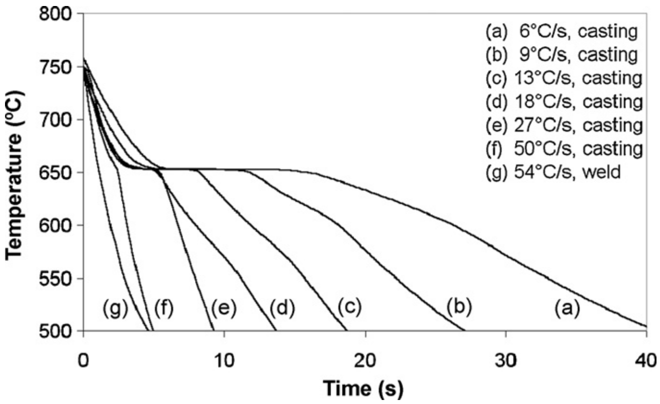

Fig. 2. Cooling curves for 6060 castings and weld metal.

4.2. Cast microstructure

From EBSD analysis, grain structure within the castings was observed to be fairly uniform and equiaxed, with average grain diameter varying from approximately 240 to 50 μm for the slowest to the fastest cooled casting. Dendrite spacing was found to vary from 50 to 14 μm for the slowest to the fastest cooling rate, which follows roughly the spacing predicted from Eq. (1) (43 and 19 μm, respectively).

With increased cooling rate there is observed an abrupt change in the structure of second phase particles that evolve during solidification of castings as shown in Fig. 3, occurring between 27 and 50 K/s. At slower cooling rates, dendrites are found outlined by a nearly continuous network of particles in Fig. 3a. At higher cooling rates, dendrites are no longer outlined by constituent phases (Fig. 3b), making dendrite boundaries harder to distinguish. Instead, constituent particles are localized in small spherical pools (1–2 μm diameter) distributed uniformly throughout each grain. Spacing between pools relates approximately to dendrite spacing, which is on the order of 14 μm for the 50 K/s cooling rate. Grain boundaries, however, remain decorated with lenticular shaped particles.

This change in phase distribution with cooling rate reflects upon the ability to nucleate and grow constituent phases. With shorter solidification times, the time available for nucleation

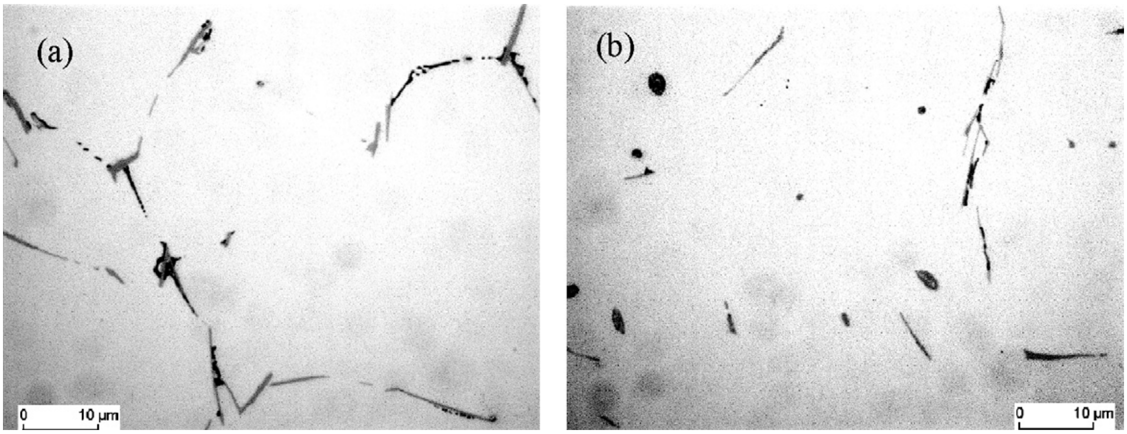

Fig. 3. As-cast 6060 microstructures for (a) 27 K/s, and (b) 50 K/s.

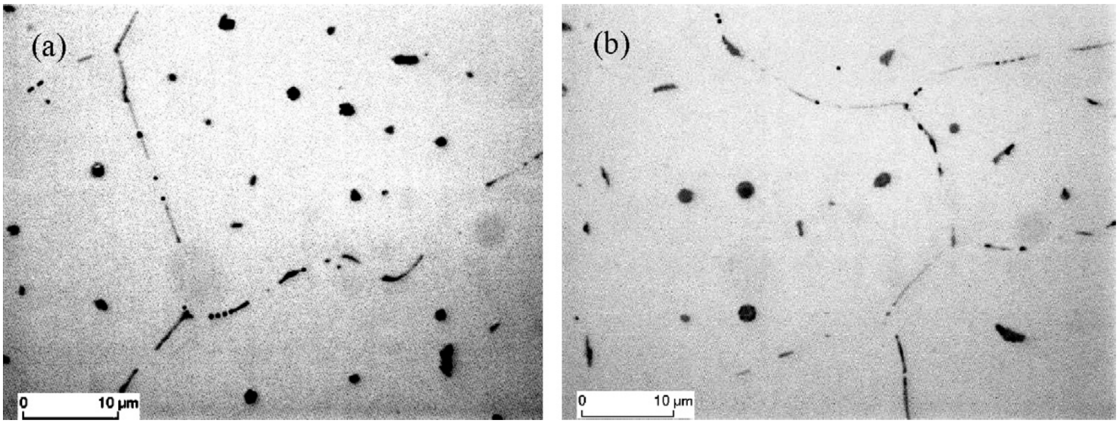

Fig. 4. Alloy 6060 weld metal microstructures for (a) 0% 4043, and (b) 16% 4043.

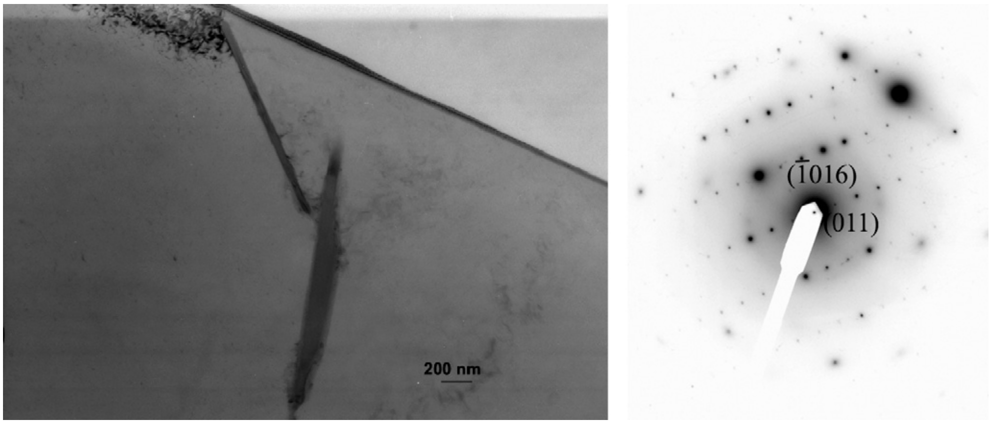

Fig. 5. TEM image and diffraction pattern for 6060 weld metal showing intergranular ß-Al_5FeSi particle.

becomes limited even though undercooling and nucleation rates are presumably higher. The time and space available for growth also becomes a limiting factor. A preferential segregation of solute to grain boundaries, however, may explain the more continuous nature of grain boundary constituents.

4.3. Weld metal microstructure

Using EBSD, grain structure in the weld metal was found to be uniform and equiaxed with average grain diameters of 51 and 63 μm for welds made with and without 4043 filler, respectively. This reflects upon a higher solidification undercooling for the weld metal with a higher Si content. Dendrite spacing was found to be approximately 14 μm for both weld types, similar to that observed for the fastest cooled casting.

Weld metal microstructure corresponding to the curve (g) in Fig. 2 is given in Fig. 4a. The addition of 4043 filler did not noticeably change the weld metal microstructure as seen in Fig. 4b, which is in stark contrast to the affect of 4043 additions to slower cooled castings (recall Fig. 1). Spherical particles of interdendritic constituents are dispersed throughout the grain, whereas grain boundaries are outlined with lenticular particles. When compared to fast cooled castings (Fig. 3b), the weld microstructures in Fig. 4 appear nearly identical, which is the result of very similar solidification conditions as determined from thermal analysis: 50 K/s cooling rate, 4 mm/s growth rate, and 12 K/mm temperature gradient.

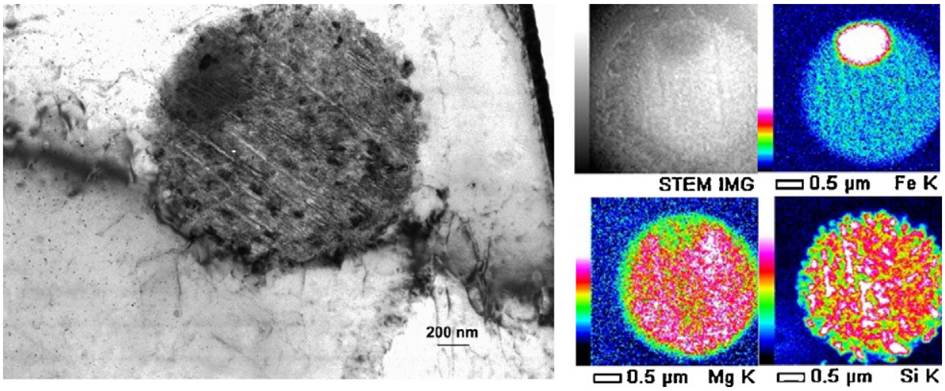

Fig. 6. TEM image of spherical particle in 6060 weld metal with corresponding STEM elemental analysis.

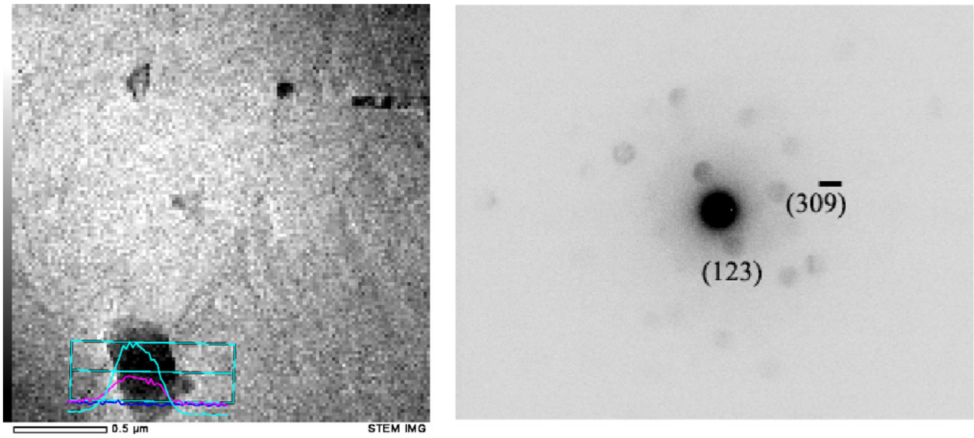

Fig. 7. TEM image and diffraction pattern for 6060 weld metal showing intragranular α-Al_8Fe_2Si particle. Line scan across particle: Fe turquoise, Si magenta.

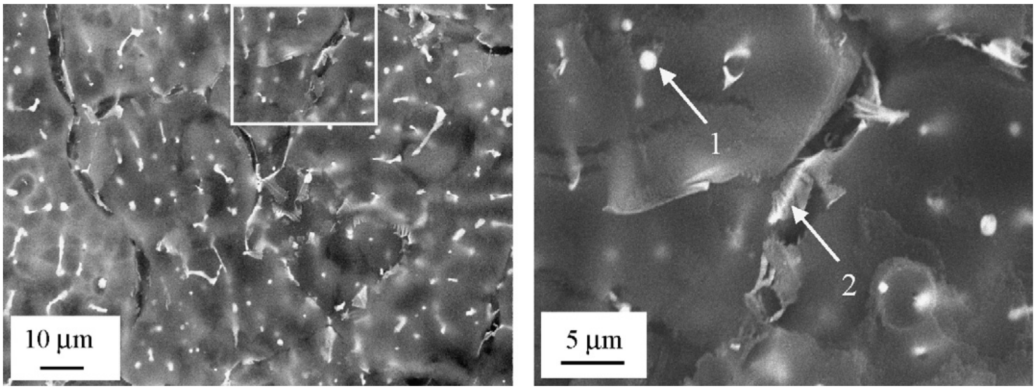

Fig. 8. EMPA analysis of deep-etched 6060 weld metal showing location of particles (1—spherical and 2—lenticular) at two magnifications, analyzed for atomic composition (see Table 3).

The grain boundary lenticular phase was positively identified using diffraction analysis to be ß-Al_5FeSi (Fig. 5). A typical intragranular spherical particle is shown in Fig. 6, and was found to contain Fe, Mg, and Si. The diffraction pattern corresponding to this particle could not be definitively indexed, suggesting that it may actually consist of a fine mixture of multiple phases. Evidence was also found for intragranular sub-micron particles of α-Al_8Fe_2Si, confirmed with diffraction analysis shown in Fig. 7. The α phase was not believed to form in the more slowly cooled 6060 castings [13].

The deep-etched specimen used for microprobe analysis is shown in Fig. 8. EPMA elemental analyses made on two types of particles (lenticular and spherical) are summarized in Table 3, showing a rough similarity with nominal ß-Al_5FeSi and π-$Al_8FeMg_3Si_6$ atomic compositions, respectively. Deviation from stoichiometric compositions likely reflects upon the local presence of multiple phases, in addition to errors caused by the abundant Al matrix phase. For example, the high Mg count in particle 1 could be due to the presence of Mg_2Si; the high Si count in particle 2 may be due to the presence of the Si phase. The complexity of phase mixtures is demonstrated by the irregular micron-sized particle shown in Fig. 9 consisting of inhomogeneous regions high in Fe + Si, Ti, and Mg.

Table 3
EPMA microprobe analysis (at.%) for particles 1 and 2 identified in Fig. 8, compared against stoichiometric phase compositions for ß, Mg_2Si, π, and Si.

Particle	Al	Fe	Mg	Si
1 (lenticular)	78	5	12	4
ß-Al_5FeSi	71	14	0	14
Mg_2Si	0	0	67	33
2 (spherical)	44	5	17	33
π-$Al_8FeMg_3Si_6$	51	30	16	2
Si	0	0	0	100

4.4. Weld thermal analysis

Fig. 10 shows results from the SS-DTA thermal analysis applied to thermocouple measurements made in weld metal. Thermal arrests were assumed associated with phase reactions (numbered 1–10) based upon work previously done for castings, examined in light of information available from the literature [13]. These reactions are summarized in Table 4, where some notable differences are observed between castings and welds. For example, a thermal arrest for α-Al_8Fe_2Si was observed for weld metal, but not for castings (i.e. reaction 4). There is evidence in the literature that fast cooling rates promote α-Al_8Fe_2Si formation at the expense of ß-Al_5FeSi [8,9,11,16,17], which supports the observation made in this study.

Also, the low melting reactions (reactions 8–10) were not observed for castings at low silicon, but were observed in low silicon weld metal. This may be due to incomplete eutectic reactions at higher temperatures (reactions 4–7) providing segregate for the low temperature reactions, as suggested by Belov et al. [9]. Note that ß needles (reaction 8) were observed only at grain boundaries, typical of low temperature segregation.

Another notable difference is that the weld metal phase reactions always occurred at slightly lower temperatures for the high silicon alloy, something not observed for castings. This suggests that these phase reactions consistently occurred at higher undercooling, perhaps due to time limited partitioning or growth of silicon. The faceted growth of silicon is known to lag behind aluminum and can

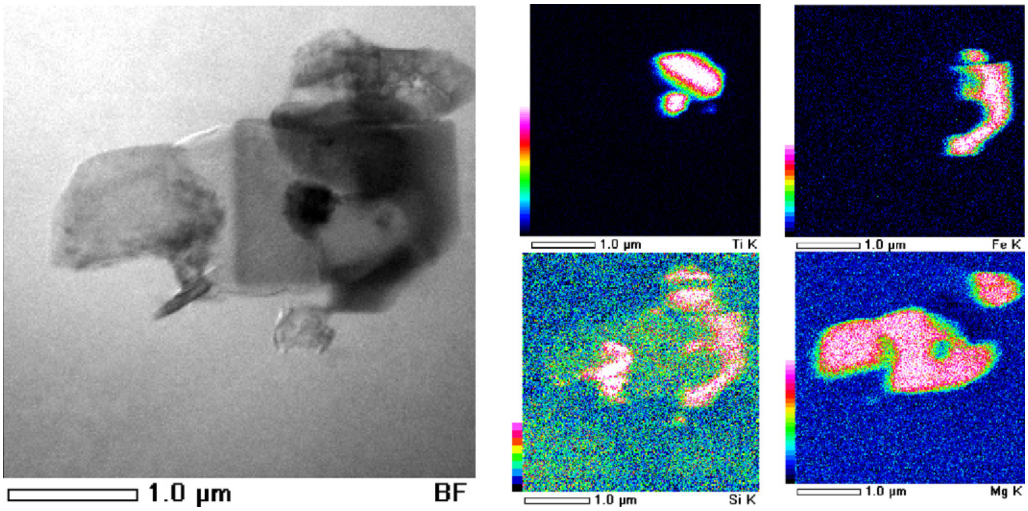

Fig. 9. TEM image of intragranular 6060 weld metal mixed-phase particle with STEM elemental analysis.

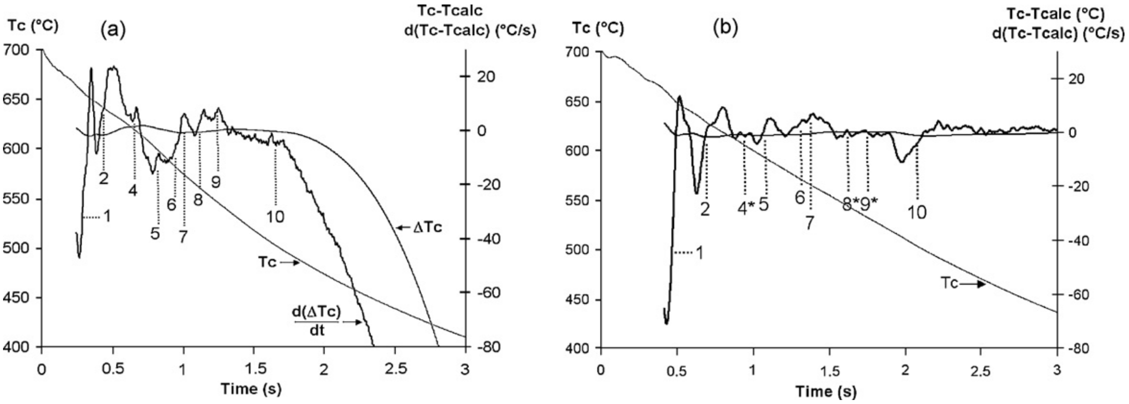

Fig. 10. SS-DTA thermal analysis of 6060 weld metal with (a) 0% 4043, and (b) 16% 4043. Arrest numbers correspond to numbered reactions in Table 4.

be modified (i.e. grown as fibers) under welding conditions [18]. The finer grain size observed for the high Si weld metal in this study also supports this argument.

The significance of these results, with regard to explaining improvements in weldability when using 4043 filler, leads one to believe that although the solidification range is largely unaffected, there is more eutectic available, particularly at grain boundaries, to feed shrinkage. This excess liquid at grain boundaries is particularly important, because this is where solidification cracking most often occurs. The rapid cooling associated with welding causes high temperature reactions to be partially suppressed (e.g. less binary ß, reaction 5), making more solute available for low temperature reactions (e.g. more ternary ß and quaternary eutectic, reactions 8 and 10) at grain boundaries. It is unlikely that the peritectic reaction (i.e. reaction 9) proceeds to any significant extent under rapid cooling conditions.

It has been suggested for castings that binary ß impairs liquid feeding, which in turn leads to porosity formation [19–22]. Regarding solidification cracking in castings, however, the general consensus is that binary ß improves resistance to cracking

Table 4

Comparison of phase reactions and thermal arrest temperatures for castings and welds. Weld data taken from SS-DTA thermal analysis in Fig. 10. Note that weld coherency point temperature (reaction 3) was determined using cooling rate method, and was not detectable from SS-DTA data.

No.	Phase reaction	Thermal arrest temperature (°C)			
		Castings at 9 K/s [13]		Welds at 54 K/s	
		6060	6060 + 20% 4043	6060	6060 + 16% 4043
1	$L + TiAl_3 \rightarrow (Al)$	666	666	660–649	659–645
2	$L \rightarrow (Al)$	653–650	650–647	646–632	636–618
3	Coherency Point	642–636	642–639	624	612
4	$L \rightarrow (Al) + \alpha(Al_8Fe_2Si)$	–	–	620–616	610–602
5	$L \rightarrow (Al) + ß(Al_5FeSi)$	609–597	–	603–596	597–587
6	$L \rightarrow (Al) + Mg_2Si$	597–587	–	587–580	580–569
7	$L \rightarrow (Al) + Si$	587–578	584–577	579–572	566–563
8	$L \rightarrow (Al) + Si + ß$	–	564–556	563–556	549–534
9	$L + ß \rightarrow (Al) + Si + \pi(Al_8FeMg_3Si_6)$	–	539–534	550–544	529–519
10	$L \rightarrow (Al) + Mg_2Si + Si + \pi$	–	524–509	507–496	511–491

[17,23,24], whereby ß needles serve to bridge across dendrites and hence reduce strain localization in the mushy state. However, in welds the ß phase is refined in size, limited to grain boundaries, and is present for both low and high 4043 additions. This suggests that this bridging mechanism does not play a role in reducing weld cracking. This hypothesis is further supported by recent weldability tests [25], where high iron variants of aluminum 6060 (up to 1.7 wt.% Fe) were found to improve castability while leaving weldability largely unaffected.

5. Conclusion

The effect of cooling rate and silicon content on 6060 solidification microstructure has been examined, including a thermal analysis of both welds and castings. When going from slow to fast cooling, there is a transition in microstructure from (i) a continuous network of interdendritic phase constituents to (ii) isolated pools of interdendritic constituents, with continuous phases only at grain boundaries. This transition occurred at a cooling rate between 27 and 50 K/s for cast 6060.

From the literature, it is expected that ß-Al_5FeSi, Mg_2Si, Si, and π-$Al_8FeMg_3Si_6$ phases should be present in cast 6060/4043 structures. Combined EPMA, STEM, and SS-DTA analyses suggest that these phases are also present in weld metal, in addition to α-Al_8Fe_2Si. Intergranualar ß-phase and intragranular α-phase were positively identified from TEM diffraction patterns. Diffraction patterns from many particles, however, could not be indexed due to their complex nature as mixtures of different phases. The intragranular spherical particles are one such example of this, although microprobe analysis supports the possible presence of the π-phase.

From thermal analysis of gas-tungsten arc welds made on 6060, an increase in weld metal silicon content, achieved by adding a 4043 filler metal, was found to have no major effect on solidification range. This is in contrast to what was found previously for slower cooled cast 6060/4043 mixtures, where silicon extended the solidification range to lower temperatures. It is believed that both an increase in silicon and faster cooling rates promote the formation of low temperature reactions at grain boundaries involving ternary ß and quaternary eutectic.

These results have direct implications regarding the cracking behavior of aluminum 6060 weld metal and associated improvements in weldability when using 4043 filler. Since 4043 filler additions do not affect solidification range or phase formation, improved weldability is more likely related to the quantity of grain boundary eutectic generated and the resulting improved ability to feed shrinkage. The formation of coarse ß particles that interlock the dendrite network and improve castability, do not exist in weld metal.

Acknowledgements

The authors are grateful to the Bundesanstalt für Materialforschung und -prüfung (BAM) for internal support of this research, and greatly appreciate the work of R. Breu for metallography, G. Oder for microprobe analysis, and R. Saliwan Neumann for EBSD analysis.

References

[1] J.H. Dudas, F.R. Collins, Weld. J. 45 (1966) 241s–249s.
[2] M.G. Mousavi, C.E. Cross, Ø. Grong, Sci. Technol. Weld. Joining 4 (1999) 381–388.
[3] M.G. Mousavi, C.E. Cross, Ø. Grong, M. Hval, Sci. Technol. Weld. Joining 2 (1997) 275–278.
[4] N. Coniglio, C.E. Cross, Weld. J. 87 (2008) 237s–247s.
[5] N. Coniglio, PhD Thesis, Otto-von-Guericke Univ. BAM Pub., Berlin, 2008.
[6] N. Coniglio, C.E. Cross, Met. Mater. Trans., in press.
[7] M. Rappaz, J.-M. Drezet, M. Gremaud, Met. Mater. Trans. 30A (1999) 449–455.
[8] P.N. Crepeau, AFS Trans. 103 (1995) 361–366.
[9] N.A. Belov, A.A. Aksenov, D.G. Eskin, Iron in Aluminum Alloys, Taylor and Francis, London, 2002.
[10] L.F. Mondolfo, Aluminum Alloys Structure and Properties, Butterworths, London, 1976.
[11] H. Tanihata, T. Sugawara, K. Matsuda, S. Ikeno, J. Mater. Sci. 34 (1999) 1205–1210.
[12] M.H. Burden, J.D. Hunt, J. Cryst. Growth 22 (1974) 109–116.
[13] N. Coniglio, C.E. Cross, Weld. World 50 (2006) 14–23.
[14] L. Bäckerud, E. Krol, J. Tamminen, Solidification Characteristics of Aluminum Alloys, vol. 1, Skanaluminium, Oslo, 1986.
[15] B.T. Alexandrov, J.C. Lippold, Trends in Welding Research, ASM International, Materials Park, 2006, pp. 975–980.
[16] C.M. Dinnis, J.A. Taylor, A.K. Dahle, Scripta Mater. 53 (2005) 955–958.
[17] L. Lu, A.K. Dahle, Met. Mater. Trans. 36A (2005) 819–835.
[18] C.E. Cross, D.L. Olson, Weld. J. 61 (1982) 381s–387s.
[19] J.E. Eklund, Helsinki University of Technology, Thesis, 1991.
[20] J.A. Taylor, G.B. Schaffer, D.H. StJohn, Proc. Int. Conf. Solidification Processing, University of Sheffield, 1997, pp. 238–242.
[21] J.A. Taylor, G.B. Schaffer, D.H. StJohn, Met. Mater. Trans. 30A (1999) 1657–1662.
[22] J.A. Taylor, C.M. Dinnis, Proc. Int. Conf. Solidification Processing, University of Sheffield, 2007, pp. 566–570.
[23] A.R.E. Singer, P.H. Jennings, J. Inst. Met. 73 (1947) 273–284.
[24] A. Couture, AFS Int. Cast Met. J. 6 (1981) 9–17.
[25] N. Coniglio, C.E. Cross, Hot Cracking Phenomena in Welds II, Springer, 2008, pp. 277–310.